Effect of Ideal, Organic Nanoparticles on the Flow Properties of Linear Polymers: Non-Einstein-like Behavior

Anish Tuteja and Michael E. Mackay*

Department of Chemical Engineering and Materials Science, Michigan State University, East Lansing, Michigan 48824

Craig J. Hawker

Materials Research Laboratory, University of California, Santa Barbara, California 93106

Brooke Van Horn[†]

IBM Almaden Laboratory, 650 Harry Road, San Jose, California 95120

ABSTRACT: The effect of nanoscopic, shape persistent polystyrene (PS) nanoparticles on the rheological properties of linear PS is studied and a dramatic viscosity reduction is observed. This is an ideal blend which simplifies enthalpic interactions between the components and can be used to delineate the effect of particle size on the properties of the blends. Homogeneous blends are assured through small-angle neutron scattering (SANS) experiments which establish the absence of phase segregation (depletion flocculation) in the nanoparticle−polymer blend. We previously found that nanoparticles reduce the viscosity of high molecular mass linear PS when the interparticle gap is smaller than the linear polymer size. In the present study, we find that such confinement of entangled polymers is necessary for the viscosity reduction since lower concentrations provide a viscosity increase. Furthermore, the behavior is found to be dependent on the presence or absence of entanglements and confinement is seemingly not important for unentangled polymers. It is proposed that constraint release caused by the addition of nanoparticles is responsible for some of the observed changes in viscosity although it is suspected this is a very complicated phenomenon and introduction of free volume by the nanoparticles is certain to play a key role.

Introduction

The terminal viscosity of polymer melts is an increasing and unique function of molecular mass (M). Below the critical mass for *entanglement coupling*[1] (M_c) the viscosity scales as M^1 while above M_c a much larger power law is evident, approximately 3.4−3.8 power[2−4] (see Figure 1; data from Fox and Flory,[2,3] Mackay and Henson,[5] and this work are included in the figure). The lower, or *Rouse*,[6] regime actually occurs over a relatively small mass range unless correction to constant fractional free volume (f) is made. The upper regime has an enhanced power law due to what has been denoted as entanglements whose physics can be described by *reptation*.[7,8] Regardless of the physical process[9] unique flow behavior occurs at M_c evidenced by the power law change.

The exact mechanism that causes entanglement coupling is not truly known, however, it is clear that the free volume is essentially constant for masses greater than M_c. Below this critical mass the free volume changes essentially in concert with the specific volume. This observation does not give a fundamental picture of the complicated polymer dynamics and merely provides empirical foundation to likely explanations that incorporate a constant free volume within an entangled polymer melt.

An interesting study was performed to elucidate how entanglements, or lack thereof, affect the flow behavior

* Corresponding author. E-mail: mackay@msu.edu. Web: www.nanoeverything.com.
† Present address: Department of Chemistry, Washington University−St. Louis, St. Louis, MO 63130.
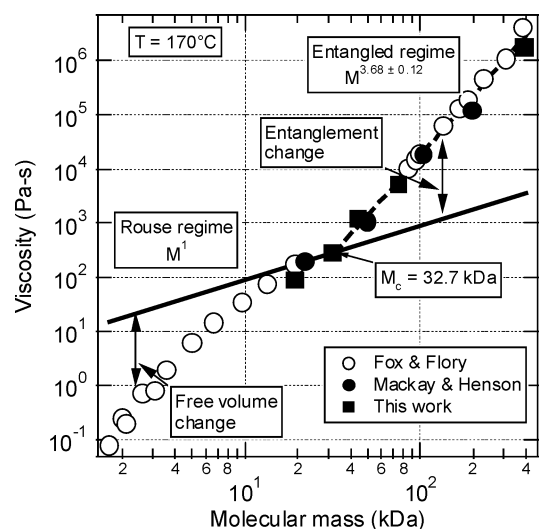
Figure 1. Viscosity as a function of molecular mass (M) for polystyrene melts at 170 °C. Data from Fox and Flory,[2,3] Mackay and Henson,[5] and this work are used to show how, below the critical molecular mass for entanglement coupling (M_c), the Rouse model is followed, except for deviations caused by a free volume change. Above M_c the entangled regime results with a much larger power law exponent of viscosity with M. Changes in the entanglement structure or dynamics could reduce the viscosity to the Rouse limit.

of polymer melts.[10] Polymer molecules were freeze-dried or crystallized from dilute solution then physically compressed and viscosity measured; no change in viscosity was found after the first 20 min, the time for the first data point to be recorded. This is in contradic-

tion to the results of Liu and Morawetz[11] who show that individual polymer molecules take an extraordinary length of time (>16 h) to reach equilibrium in a melt. However, Farrington[12] determined that the storage modulus (G') changed significantly within the first 20 min for samples prepared similar to above or for microemulsion polymerized polystyrene nanoparticles that were allowed to interdiffuse upon heating (particle size ∼ 40 nm, M ∼ 10^6 Da). This process depended on temperature and when compared to the relaxation or reptation time (t_d) approximately $10t_d$ was required for equilibrium. Although this study could follow the kinetics of entanglement formation, the true equilibrium, in accord with the work of Liu and Morawetz, was not achieved suggesting polymer melts are either never at true equilibrium and/or flow properties are not sensitive to nonequilibrium structure.

Despite the apparent difficulty in robustly degrading entanglements through physical means one can eliminate them through flow.[13] Shear can reduce entanglements or constraints,[14] and as shown in Figure 1, the possible change in viscosity to the free Rouse chain limit exemplifies the overall effect of entanglements. If entanglements could be eliminated by solution precipitation techniques one would expect the Rouse limit to similarly apply.[8]

It is conjectured that thin polymer films next to hard surfaces[15,16] change polymer entanglement[17] with minimal change in the radius of gyration (R_g) parallel to the substrate.[18] So it was hypothesized by us that nanoparticle inclusion could affect polymer flow in a more robust manner compared to precipitation techniques discussed above due to the introduction of a vast number of hard surfaces by the nanoparticles. Yet, addition of particulates to polymer melts demonstrates complicated behavior,[19] although continuum relations provide methods to data correlation. In Einstein's seminal manuscript,[20] it was shown that the viscosity increase Brownian particles provide scales with the particle volume fraction, ϕ ($\eta = \eta_s[1 + 2.5\phi]$, where η is the solution viscosity and η_s is the solvent viscosity). A viscosity increase has been observed in many systems[21] even when small (∼260 nm) polystyrene latex particles[22] and nanoparticles (∼56 nm) made of silica[23] were studied. These systems have particle sizes much larger than the suspending fluids' molecular size and so continuum expectations introduced by Einstein are followed.

Of course, when the particle becomes molecular in size it is possible to see deviations. Edward[24] surveyed the literature to find when the Stokes–Einstein (SE) relation could not be applied to diffusion of molecular penetrants in simple fluids such as water and carbon tetrachloride. When the penetrant's radius (a) became 2–3 times that of the suspending liquids' then deviations from the SE relation were evident. This is equivalent to stating that the numerical factor for the friction coefficient ζ ($\equiv 6\pi\eta_s a$) is no longer 6 and decreased in value when very small penetrants were considered.

Deviations from the SE relation have been observed in diffusion of tracer spheres in polymer solutions.[25] In this case, however, the most significant deviation occurred at high polymer concentration with large spheres (a ∼ 1 μm) rather than smaller (a ∼ 20 nm). The explanation given was that shear thinning influenced the diffusivity. More recent work has concentrated on this effect to determine the microrheology or local viscosity of polymer solutions (see e.g. Lu and So-

lomon[26]). This phenomenon is argued as related to local scale heterogeneity of the polymer solution. Furthermore, larger particles were found to diffuse faster than smaller and this may be akin to the principle of size exclusion chromatography as the larger particles take a less circuitous route through the heterogeneous structure.

The situation is different in polymer melts such as poly(dimethylsiloxane) or PDMS. Roberts et al.[27] showed that a larger silicate nanoparticle ($a = 2.8$ nm) followed the SE relation as long as an adsorption layer of PDMS was considered. The 5 kDa polymer's radius of gyration (R_g) was 2.0 nm and so the particle and polymer were of the same size. Of course, the particle is much larger than the PDMS monomer unit. When a smaller nanoparticle was investigated ($a = 0.44$ nm), which is closer in size to the monomer unit and much smaller than the polymer as a whole, anomalous behavior was observed and the particle appeared smaller than its true size, at least in a hydrodynamic sense. The authors state that this smaller nanoparticle behaved like a solvent while the larger as a colloidal particle. Note M_c for PDMS is 24.5 kDa[1] and so all the studies by Roberts et al. were conducted in an **unentangled** polymer melt.

Recently, Zhang and Archer[28] studied the effect of the nanoparticle–polymer interaction parameter, in blends of poly(ethylene oxide) (PEO) and silica nanoparticles (∼12 nm diameter). Pure silica nanoparticles are strongly interacting (physisorption) with PEO. It was seen that even a very small addition of nanoparticles caused a large increase in viscosity of an **entangled** PEO system, probably by formation of a polymer-nanoparticle network in the melt. When the nanoparticle surface was chemically modified by grafting an oligomeric PEO terminated with a trimethoxy silanyl group, no network formation was found. Furthermore, there was no change in the viscosity of the polymer melt on nanoparticle addition.

The above provides a brief introduction to the complicated dynamics of polymer melts and highlights that the size and scale of nanoparticles compared to polymer molecules could yield interesting behavior. The nanoparticles used in this work have a size between 5 and 10 nm which is much larger than a monomer unit (∼0.3 nm). Polymers in contrast to simple fluids, like water, have an equilibrium configuration that spans 10–20 nm and so the nanoparticles are smaller than the polymer molecules. Furthermore, the size associated with entanglement coupling is approximately 5–10 nm and is of the same size as the nanoparticles. Clearly, the nanoscopic size chosen here could disrupt the polymer dynamics.

In our previous study,[29] we investigated the effect of polystyrene nanoparticles[30] on the flow properties of **entangled** polystyrene melts. This is an ideal system since the particle and polymer are chemically equivalent, and have a similar refractive index, thereby reducing if not eliminating dispersion forces.[31] Thus, the system was equivalent to hard spheres dispersed in an entangled polymer melt.

The terminal (zero shear) viscosities of the systems were always found to decrease upon nanoparticle addition, paralleling the reduction of the glass transition temperature (T_g). The plateau modulus (G_N^0) was not affected and so it was argued that the entanglement density[1,8] was not affected. Furthermore, a graph of the terminal viscosity with temperature (T) above T_g, or T

$- T_g$, resulted in a master curve suggesting that the nanoparticles caused a glass transition temperature decrease and the viscosity reduction related to a free volume change. Evidently the free volume change of unentangled melts, concomitant with the excess viscosity reduction below the Rouse limit, is translated to entangled melts (see Figure 1).

Free volume could be readily incorporated by nanoparticles through their high surface area-to-volume ratio.[32] Assuming an excluded volume layer of thickness Δ exists around each nanoparticle, the fractional free volume (f) within the linear polystyrene matrix is increased by $\sim 3\phi\Delta/a$. The free volume increase can be quite large for nanoparticles; assuming a volume fraction of 0.1, exclusion layer thickness of 0.1 nm and radius of 3 nm results in an f increase of 0.01 which is a 10−20% increase in free volume at typical melt temperatures. A colloidal scale particle ($a \sim 300$ nm) produces a much smaller fractional free volume increase, 0.0001.

It was anticipated by Mackay et al.[29] that the viscosity decrease was a much more complicated phenomenon than a mere free volume increase. This became evident when the average interparticle half gap (h) was determined. Twice this distance represents the average distance separating particles and is approximated by

$$h/a = [\phi_m/\phi]^{1/3} - 1 \qquad (1)$$

where ϕ_m is the maximum random packing volume fraction (~ 0.638). Since the half gap scales with nanoparticle radius, this variable can become quite small at modest loadings. For example, a 3 nm radius nanoparticle at a volume fraction of 0.1 suspended in a liquid results in an average half gap of ~ 2.5 nm and is much smaller than the entangled linear polymer's R_g. Thus, it appears easy to confine linear polymers between nanoparticles at moderate volume fractions as long as they do not agglomerate (depletion flocculation). The systems discussed by Mackay et al. were all confined (i.e. $h < R_g$) and the linear polymer had masses above M_c.

We were able to confirm through small-angle neutron scattering (SANS) that our system did not significantly agglomerate even at volume fractions of 0.5. This result agrees with Cosgrove et al.'s study[33] for a poly(ethylene oxide)−water system containing silica nanoparticles ($a = 8$ nm). They found that negligible particle clustering was evident possibly because the nanoparticles are smaller than the linear polymer ($R_g \sim 10-35$ nm). It can be hypothesized that continuum arguments[34] are no longer valid in nanosystems and when R_g/h approaches and exceeds one phase separation and agglomeration does not occur. Indeed this will be addressed in a future publication by us.

In the present study we extend our results to gain further insight into this unique phenomenon of a viscosity reduction when nanoparticles are added to polymer melts. The ratio R_g/h was greater than one in the previous study[29] indicating that the linear macromolecules in the continuous phase were always confined. Here the ratio is made less than one to determine the effect of this variable under different conditions. In addition, a wider range of nanoparticle sizes and polymer molecular masses are used to elucidate the effect of size and molecular architecture on the flow properties of polymer melts.

Table 1. Polystyrene Materials Used in This Study

sample	M_w (kDa)[a]	M_n (kDa)[a]	condition
PS 19kDa	19.3	18.1	linear
PS 31kDa	31.6	28.9	linear
PS 75kDa	75.7	64.7	linear
PS 393kDa	393.4	339.1	linear
d-PS 155kDa	155.8	130.9	linear
25 kDa NP	27.3[b]	25.3[b]	cross-linked
52 kDa NP	61.3[b]	52.0[b]	cross-linked
135 kDa NP	162.0[b]	135.0[b]	cross-linked

[a] M_w is the weight-average mass and M_n is the number-average molecular mass. [b] On the basis of the assumption that a single chain collapses to give a single nanoparticle. The masses for the linear chains were determined by GPC.

Experiment

Materials and Synthesis. Linear polystyrene (PS) was purchased from Scientific Polymer Products at molecular masses of 19.3, 31.6, 75.7, and 393.4 kDa. Details of these polymers are given in Table 1. The radius of gyration was determined by a relation developed from data of Cotton et al.[35] (R_g (nm) = 0.87 $\sqrt{M}$ (kDa), a deuterated polymer has a prefactor of 0.84) The nanoparticles (NPs) were synthesized by intramolecular cross-linking, details of the process are provided elsewhere.[30] All the nanoparticles used in this work were tightly cross-linked (20 mol % intramolecular cross-linking). It should be pointed out that the solubility parameter for the polystyrene nanoparticles matched that for linear polystyrene (9.1−9.2 (cal/cm^3)$^{1/2}$) determined by measuring the hydrodynamic radius in various solvents via dynamic light scattering. The solvent producing the largest radius is assumed to have the same solubility parameter as the polymer. All solvents were purchased from Sigma-Aldrich and used as received.

Sample Preparation. Blends of the PS nanoparticles with linear PS were prepared through co-dissolution in THF and rapid precipitation with methanol,[29,36] followed by drying in a vacuum at 50 °C for at least a week to ensure complete solvent removal. The powder was then molded by compression, under vacuum, in a pellet press (8 mm diameter) to ensure that no trapped air remained in the sample. The samples were aged at 130−170 °C, under vacuum, for several hours to ensure homogeneity.

Rheology Measurements. The 8 mm diameter disks obtained from the pellet press were placed on the 8 mm parallel plates fixture of a Rheometrics ARES rheometer set at a gap of approximately 0.4 mm. Measurements were done in the dynamic (oscillatory) mode. Frequency sweeps in the range 0.1−100 rad/s were performed at various temperatures. These were then combined using time−temperature superposition[37] to yield a master curve at 170 °C (all quoted temperatures refer to the surface temperature of the lower plate). The strain during the dynamic shear test was kept small enough to ensure that all response was in the linear viscoelastic region. A dwell time of 8−10 min was allowed at each temperature for the samples to attain a uniform melt temperature, before commencing measurements.

Differential Scanning Calorimetry (DSC) Measurements. A TA instruments Q-1000 DSC was used to perform all glass transition measurements. Each sample was subjected to at least three heating − cooling cycles, where each cycle consisted of heating the sample from 0 to 200 °C, at a rate of 5 °C/min, followed by cooling back to 0 °C, also at 5 °C/min. The inflection point for the heat flow as a function of temperature was taken as the glass transition temperature for a particular cycle. The glass transition temperatures reported in this work are the mean of the glass transition temperatures obtained from the second and the third run cycle.

Relaxation Spectra. The RSI Orchestrator software available with the ARES rheometer was used to evaluate the continuous relaxation spectra, using both the G' (storage modulus) and G'' (loss modulus) data. An algorithm developed by Mead[38,39] was used to model the relaxation modulus as a
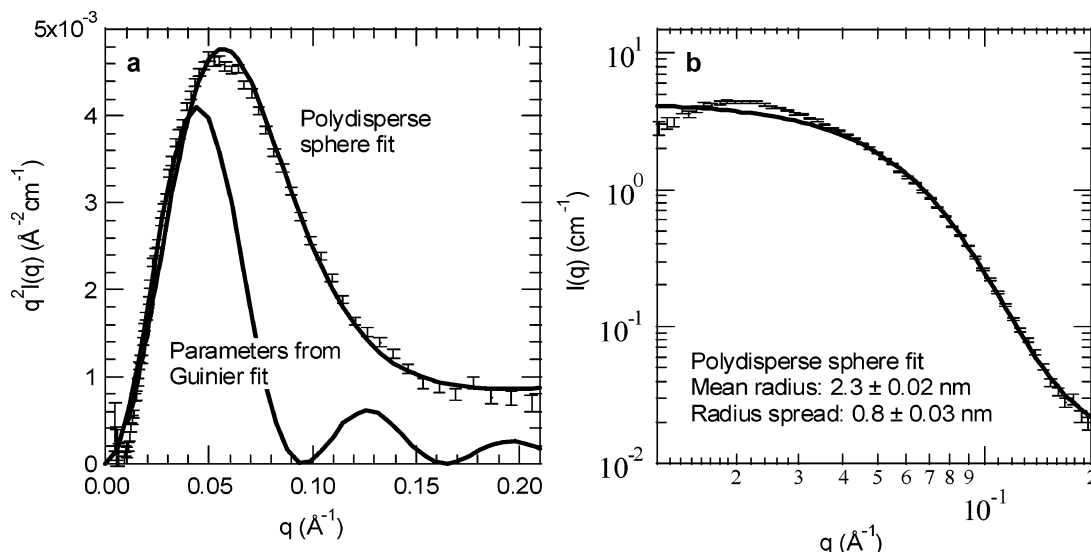
Figure 2. (a) Neutron scattering intensity (I) multiplied by the wave vector (q) squared as a function of wave vector (Kratky plot) for 2 wt % 52 kDa NP blended with d-PS 155 kDa. The peak is associated with globular objects and the associated Schulz polydisperse hard sphere fit reasonably represents the data (mean radius of $2.3 \pm 0.0_2$ nm with a radius spread of $0.8 \pm 0.0_3$ nm). The other curve is the result of a simulation assuming a monodisperse system of spheres with a radius given by the Guinier result (4.0 nm = $\sqrt{(5/3)} \times 3.1$ nm). (b) The log−log graphs of intensity vs wave vector for the same system and the associated polydisperse hard sphere fit.

discrete N element Maxwell line spectrum. In such a case the storage and loss moduli for a system are given as

$$G'(\omega) = \sum_{i=1}^{N} G_i \frac{(\omega t_i)^2}{1 + (\omega t_i)^2} \tag{2a}$$

$$G(\omega) = \sum_{i=1}^{N} G_i \frac{\omega t_i}{1 + (\omega t_i)^2} \tag{2b}$$

where ω is the frequency, t_i are the time constants, and G_i are the corresponding moduli. The discrete relaxation spectra are converted to a continuous relaxation spectrum based on the work of Baumgaertel and Winter.[40] They developed the "parsimonious" model to mimic a continuous relaxation spectrum, based on the idea that the discrete relaxation times should be freely adjustable so as to converge to the characteristic relaxation values for the material under study. Then, for a system having equally log-spaced time constants, the continuous $H(t_i)$ and the discrete spectra are related by a simple scale factor

$$G_i = H(t_i) \log(R) \tag{3}$$

where R is the ratio of successive time constants.

Small-Angle Neutron Scattering (SANS). The SANS experiments were performed on the compression molded samples at the SAND instrument of IPNS at Argonne National Laboratory.[41] Neutrons are produced at IPNS with a pulse frequency of 30 Hz and wavelengths (λ) in the range 1.4−14 Å. The instrument has a fixed detector distance of 2 m, which results in an instrument q range of 0.005−0.6 Å^{-1} ($q = 4\pi/\lambda \sin(\theta/2)$, where θ is the scattering angle). The instrument detector was a 40×40 cm^2 area sensitive ^{3}He detector with 128×128 channels. The scattering time for the samples was 2 h.

The raw data were absolutely calibrated using a silica standard, following the described procedure at IPNS.[42] All samples were also run in transmission mode for 15 min to aid in the calibration.

Kratky Plots. The description of scattering from polymer chains in their theta condition (second virial coefficient, $A_2 = 0$) was first postulated by Debye.[43] For a Gaussian distribution

of segment density within the coil the scattering function (or differential cross-section) $I(q)$ is given as[44,45]

$$I(q) = \phi \times V(\Delta\rho)^2 \{2(\exp(-(qR_g)^2) + (qR_g)^2 - 1)/(qR_g)^4\} \tag{4}$$

Here, ϕ is the volume fraction of scattering centers, V, the volume of a single scattering center and $(\Delta\rho)^2$, the difference in the scattering length densities between solvent and scatterer (or the contrast). In the high q limit (practically $q > 5R_g^{-1}$),[44] eq 4 reduces to

$$I(q) \times q^2 = 2\phi \times V(\Delta\rho)^2/(R_g^2) \tag{5}$$

The plot showing the variation of $I(q) \times q^2$ with q is known as a Kratky plot. For any given sample, ϕ, V, $\Delta\rho$, R_g are constant, thus, from eqs 4 and 5, for an ideal, Gaussian coil the Kratky plot should asymptotically approach a constant value (plateau) at high q values.

The Kratky plot is a good indicator of the polymer's inherent molecular architecture as it reflects the short-range interactions acting along the polymer chain from neighbor to neighbor, such as bond forces and hindrance of rotation. Deviations from the asymptotic behavior (as observed for a polymer coil) in the Kratky plot indicates nonideal arrangement of the polymer segments. A constant density sphere has no plateau and a series of ever decreasing peaks is seen. Both ring and star polymers have a peak (maximum) prior to the asymptote revealing different distributions than linear polymers.[46]

Results and Discussion

SANS serves as an important tool to determine the degree of dispersion as well as the molecular architecture of polymer nanoparticles, both in solution and in melt states. This technique is especially useful for this system as there is no optical or mass contrast between the PS nanoparticles and linear PS, eliminating the possible use of light or X-ray scattering, as well as electron microscopy, for characterization.

Figure 2a shows the Kratky plot for a 2% blend (by mass) of the 52 kDa NP in deuterated-155 kDa linear polystyrene. The background was deuterated-polysty-
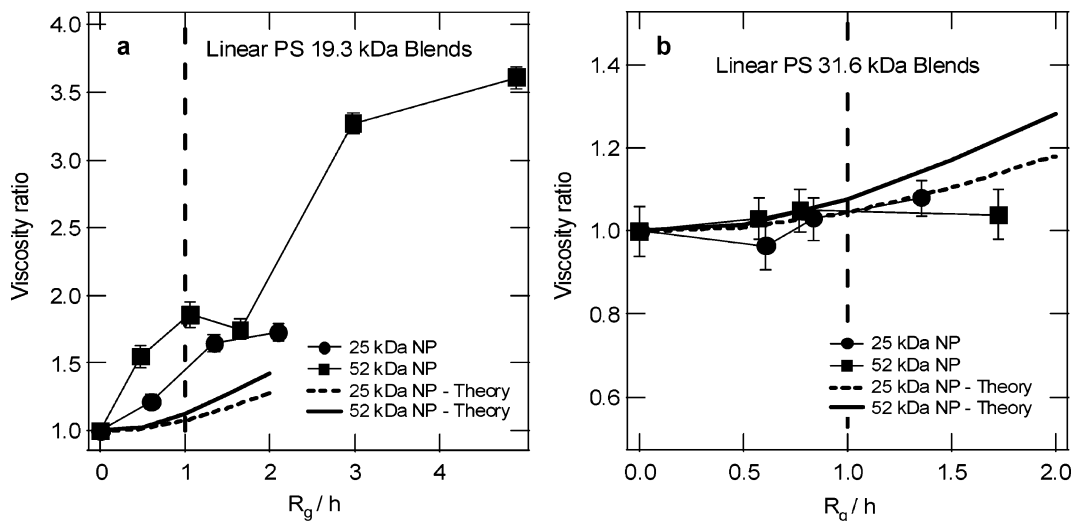
Figure 3. Viscosity ratio of the nanoparticle blends with respect to pure polystyrene, with polystyrene below (19.3 kDa) (a) and near (31.6 kDa) (b) the critical entanglement molecular mass at 170 °C. The curves labeled theory are the values predicted by Batchelor's relation for this system, ending at the limit of the relation's applicability ($\phi \sim 0.1$). It can be seen that the blend viscosity is much greater than the predicted value for the blends below M_c, however, when the polymer is near M_c, the viscosity hardly varies with addition of nanoparticles, again contradicting the Einstein and Batchelor predictions.

rene, and hence the data show scattering from the nanoparticles. The peak in the Kratky plot is immediately apparent, indicating that the intramolecular cross-linking induces a particle like nature to the molecules.[47]

Figure 2b shows the scattering intensity from the same sample as a function of the wave vector q. It can be seen that the intensity is not a power law function of q, instead the intensity goes to a plateau in the low q regime, confirming the absence of phase separation (depletion flocculation) of the nanoparticles, which has been a common problem with other nanoparticle–polymer blends.[48,49]

Also, shown in Figure 2a, is the Kratky profile for a monodisperse hard sphere system having the same radius of gyration as the nanoparticles determined with the Guinier technique. The Guinier approximation is applied in the low q scattering regime, when $q \times R_g$ is small and can be written as

$$\log I(q) = \log I(0) - \frac{(qR_g)^2}{3} \qquad (6)$$

where $I(0)$ is given by $\phi V(\Delta\rho)^2$. The Guinier plot,[50] log-$(I(q))$ vs q^2, allows determination of R_g and, furthermore, can be used as a concentration check through the neutron intensity at zero wave vector, which we have done.

The parameters determined from the Guinier fit do not represent the data well due to the slight sample polydispersity. This becomes apparent when the scattering data are fitted to a polydisperse hard sphere model by assuming a Schulz distribution[51] arriving at a mean radius ($\langle a \rangle$) of $2.3 \pm 0.0_2$ nm and a radius spread of $0.8 \pm 0.0_3$ nm; the fit is shown in Figure 2 to be reasonably representative of the data. These values yield a radius polydispersity index (rPDI) of 1.12 and polydispersity parameter of 8.3 (k, rPDI = $[k + 1]/k$). The z-average radius can be found to be 2.9 ± 0.6 nm ($[k + 2]/k \times \langle a \rangle$) while the radius found from the Guinier analysis is 4.0 ± 0.9 nm (for a hard sphere $a = \sqrt{(5/3)} \times R_g$). Since the Guinier technique yields the z-average size, agreement between these two values is expected,

while deviations between them may occur from errors in either regression and/or because the polydispersity is not accurately described by the Schulz distribution. Polydispersity is expected through the nature of the polymerization reaction as well as the cross-linking process itself which may produce molecular dimers, trimers, etc. We use a radius calculated from the expected number-average molecular mass for the NPs (Table 1) assuming a density (1.04 g/cm³) equivalent to bulk polystyrene.

Since homogeneous blends can be produced, different molecular mass nanoparticles were blended with linear polystyrene having molecular mass below M_c (unentangled), near M_c and above M_c (entangled). Figure 3a shows the ratio of the terminal (zero shear) viscosity of the nanoparticle blends with PS 19.3 kDa to the terminal viscosity of pure PS 19.3 kDa, as a function of R_g/h (see eq 1). When the ratio R_g/h is less than 1, the interparticle separation between the nanoparticles is greater than the radius of gyration of the linear polymer coil. With increasing particle loading, the interparticle gap becomes less than the radius of the polymer, causing confinement. It is important to point out that none of the viscosity data discussed here show a master curve when correlated with particle volume fraction (see Appendix).

From Figure 3a, it can be seen that addition of both the 25 and the 52 kDa nanoparticles causes a sharp increase in the viscosity of the polymer melt. The curves labeled "theory" are predictions from Batchelor's relation,[52] which is a modification of Einstein's relation, and includes the effect of hydrodynamic interactions in the system with increasing concentration

$$\eta = \eta_s(1 + 2.5\phi + 6.2\phi^2) \qquad (7)$$

The ϕ^2 correction improves the limit of applicability of Batchelor's relation to $\phi \sim 0.1$ as compared to Einstein's relation, whose limit is $\phi \sim 0.02$. From Figure 3a, it can be seen that addition of nanoparticles increases the viscosity of unentangled polymers and this increase is much greater than predicted by either Einstein or Batchelor. Also, the increase in viscosity caused by the
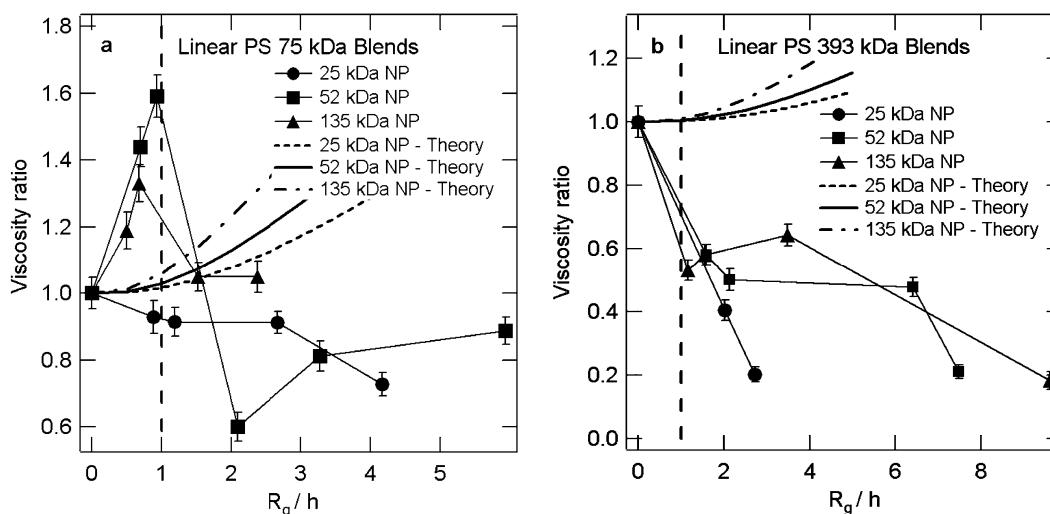
Figure 4. Viscosity ratio of the nanoparticle blends with respect to pure polystyrene for two different entangled systems, PS 75 kDa (a) and PS 393 kDa (b) at 170 °C. The curves labeled theory are the values predicted by Batchelor's relation and these end at the limit of the relation's applicability ($\phi \sim 0.1$). The viscosity falls precipitously when the radius of gyration is greater than the interparticle half-gap for the entangled systems.

addition of 52 kDa NP's is greater than caused by the 25 kDa NP's, suggesting that the viscosity increase in the polymer is affected by nanoparticle size.

Figure 3b shows the effect of nanoparticle addition on linear polystyrene near M_c. In this case it can be seen that there is essentially no change in the viscosity of the linear polymer on the addition of nanoparticles, even with particle volume fractions as high as 0.1 (the standard deviation in the measured viscosity for all samples was < 5%). This surprising result holds true for both the 25 kDa and 52 kDa nanoparticles. It was also seen that the complex viscosity (η^*), storage modulus (G') and loss modulus (G'') curves (not shown here) for all the nanoparticle blends completely overlaid with the pure linear polymer curve at all frequencies. This observation is in stark contrast to what is seen for the unentangled and the entangled polymers, as will be shown below.

Entangled polystyrene samples with molecular mass 75 and 393 kDa, were blended with the nanoparticles at various concentrations, and as shown in Figure 4a, the viscosity ratio for PS 75 kDa is a complicated function of R_g/h. It is immediately apparent that the behavior of the entangled system is different to the previous two cases that were considered. For both the 52 kDa and the 135 kDa NP it can be seen that when R_g/h is less than 1 (no confinement), the viscosity increases sharply. Here the increase in viscosity is much greater than that predicted by either Einstein's or Batchelor's relation. However, as soon as R_g/h is greater than 1 (confinement), there is an abrupt decrease in viscosity. For example, the 52 kDa nanoparticle system has a viscosity ratio change from 1.6 to 0.6 as the R_g/h value changes from 0.9 ($\phi = 0.01$) to 2.1 ($\phi = 0.05$). In all the different nanoparticle systems, for values of R_g/h greater than one, it can be seen that the viscosity ratio is either close to 1 or is greatly reduced. Thus, the confinement of the linear chain leads to a reduction in the melt viscosity, even as the particle volume fraction is increased. It is also important to point out the reduction in viscosity does not scale with the volume fraction (see Appendix) of the added nanoparticles, as mentioned above. This suggests that the mixing rule for viscosity is not applicable for this system.

The viscosity variation for the PS 393 kDa blends is shown in Figure 4b. In this case all the blends considered had an R_g/h value >1, and as was seen for the PS 75 kDa blends, the viscosity is decreased for all the nanoparticle blends at all concentrations. It is interesting to note addition of just 1% ($R_g/h = 2.8$) of the 25 kDa NP causes an 80% reduction in the melt viscosity. It was difficult to produce a blend with R_g/h <1 for this system because of the very low concentration of nanoparticles required.

The complex viscosity profiles for the pure polystyrene (PS 393 kDa), pure 52 kDa nanoparticles, as well as their blends, as a function of frequency, are presented in Figure 5a. It is observed that the pure nanoparticle system does not have a terminal viscosity and instead behaves like a yield stress material, having an infinite viscosity at zero shear rate (frequency). This behavior is similar to the rheological behavior of some intramolecularly cross-linked polystyrene microgels studied by Antonietti et al.[53,54]

In contrast, both the pure linear polymer and the nanoparticle blends have a finite terminal viscosity. From Figure 5a, it can also be seen addition of nanoparticles at low concentrations (up to $\phi \sim 0.08$), only affects the terminal region, demonstrated by a lower zero shear viscosity. Above a critical frequency ($\sim 10^{-1}$ rad/s in this case) the viscosity curves for all the blends merge with the pure polystyrene curve. However, further addition of nanoparticles causes a viscosity reduction at all frequencies, as can be seen with the 10% blend.

The same trend is observed for the storage modulus curves of the pure components and the blends (Figure 5b). Traditionally the storage modulus for the polymer blends relates directly to the storage modulus of its components.[55,56] In this case, however, G' variation for the blends is governed by the G' for the linear polymer, with the nanoparticles providing a reduction in the terminal region. As was seen earlier, after a frequency $\sim 10^{-1}$ rad/s, all the G' curves (up to $\phi \sim 0.08$) merge with the pure PS 393 kDa curve.

For all the blends discussed above, the minima in G''/G' (tan δ) occurred near a frequency of 10 rad/s. The value of G' corresponding to the minima in tan δ is
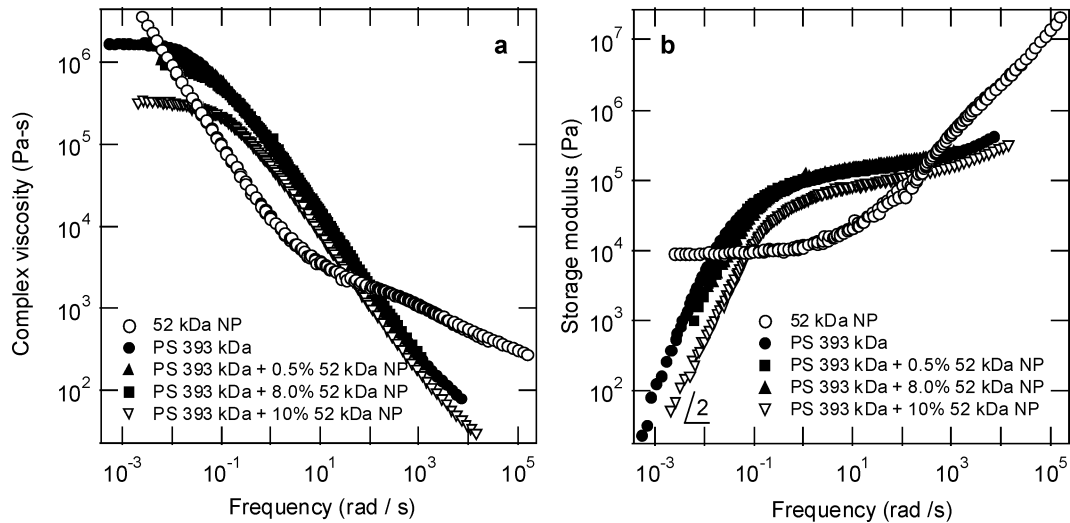
Figure 5. (a) Complex viscosity as a function of frequency for PS 393 kDa, 52 kDa NP and their blends at 170 °C. It can be seen that the pure nanoparticles display a gel like behavior with an infinite terminal viscosity. All the blends however have a distinct terminal viscosity which is lower than the pure component. (b) Storage modulus variation with frequency for the same systems at 170 °C. Blends with a nanoparticle concentration below 10% have a plateau modulus equivalent to the virgin polymer while the 10% blend has a reduced modulus and complex viscosity at all frequencies.

Table 2. The Plateau Modulus for Pure PS 393 kDa and Its Blends with Various Nanoparticles at 170 °C

| sample	plateau modulus (MPa)
PS 393 kDa	0.167 ± 0.015
PS 393 kDa + 25kDa NP −0.5% blend	0.165 ± 0.019
PS 393 kDa + 25kDa NP −1% blend	0.078 ± 0.009^a
PS 393 kDa + 52kDa NP −0.5% blend	0.171 ± 0.009
PS 393 kDa + 52kDa NP −1% blend	0.161 ± 0.020
PS 393 kDa + 52kDa NP −8% blend	0.180 ± 0.014
PS 393 kDa + 52kDa NP-10% blend	0.103 ± 0.005^a
PS 393 kDa + 135kDa NP-0.5% blend	0.192 ± 0.016
PS 393 kDa + 135kDa NP-1% blend	0.184 ± 0.014
PS 393 kDa + 135kDa NP-20% blend	0.061 ± 0.015^a

^{a} The viscosity for these blends was reduced at all frequencies on nanoparticle addition, as compared to the neat polymer.

taken as the plateau modulus (G_N^0).[57] As all the G' curves overlay near this frequency, it was concluded that the plateau modulus of the polymer is unaffected by addition of nanoparticles, up to $\phi = 0.08$ (the G_N^0 values are listed in Table 2). This observation is

contrary to the rule of mixing for athermal systems as postulated by both Tsenoglou[58] and Wu,[59] where the plateau modulus for the blend scales with the plateau modulus of its components.

It is interesting to compare the effect of nanoparticle size on the complex viscosity profile for PS 393 kDa. Addition of 52 kDa NP ($R_g = 3.1$ nm; Figure 5a) caused an effect only in the terminal region at low volume fractions with a decreased viscosity at all frequencies at higher volume fractions ($\phi \sim 0.1$). In comparison, the addition of 25 kDa NP ($R_g = 2.2$ nm) causes a decrease in viscosity at all frequencies with particle volume fractions as low as 0.01, as shown in Figure 6a. The addition of 135 kDa NP ($R_g = 4.0$ nm, Figure 6b), again affects only the terminal region at low volume fraction, while at higher volume fractions ($\phi \sim 0.2$), the viscosity is decreased at all frequencies. Note the polymer is confined for all these systems, i.e., $R_g/h > 1$.

This differing viscosity behavior can be related to the total number of nanoparticles present in the blend, at
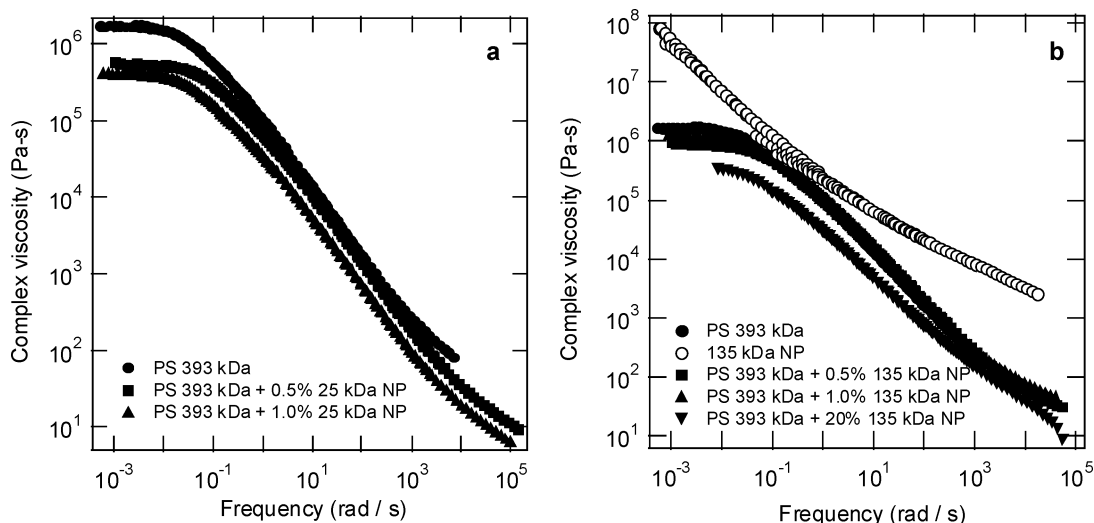
Figure 6. (a). Complex viscosity as a function of frequency for pure PS 393 kDa and its blends with 25 kDa NP at 170 °C. In this case, the viscosity is decreased at all frequencies. A large viscosity reduction is apparent with just 1% addition of the nanoparticles. (b) Complex viscosity as a function of frequency for the blends of 135 kDa NP with PS 393 kDa also at 170 °C. Here, only the terminal viscosity is reduced with nanoparticle addition until the concentration reaches 20%.
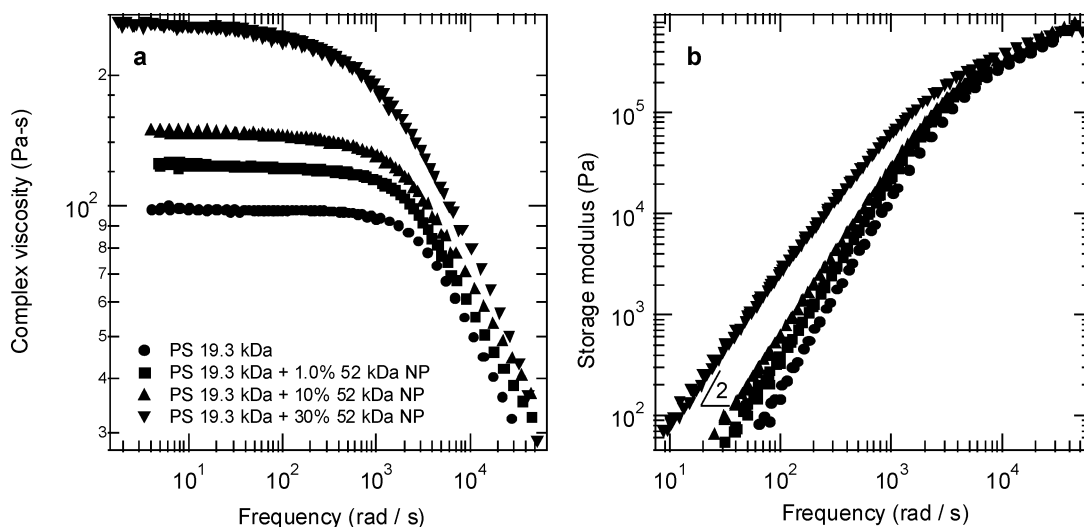
Figure 7. Complex viscosity (a) and storage modulus (b) data for pure PS 19.3 kDa and its blends with 52 kDa NP at 170 °C. Both these properties increase at all frequencies upon nanoparticle addition. Same symbols used in each graph.
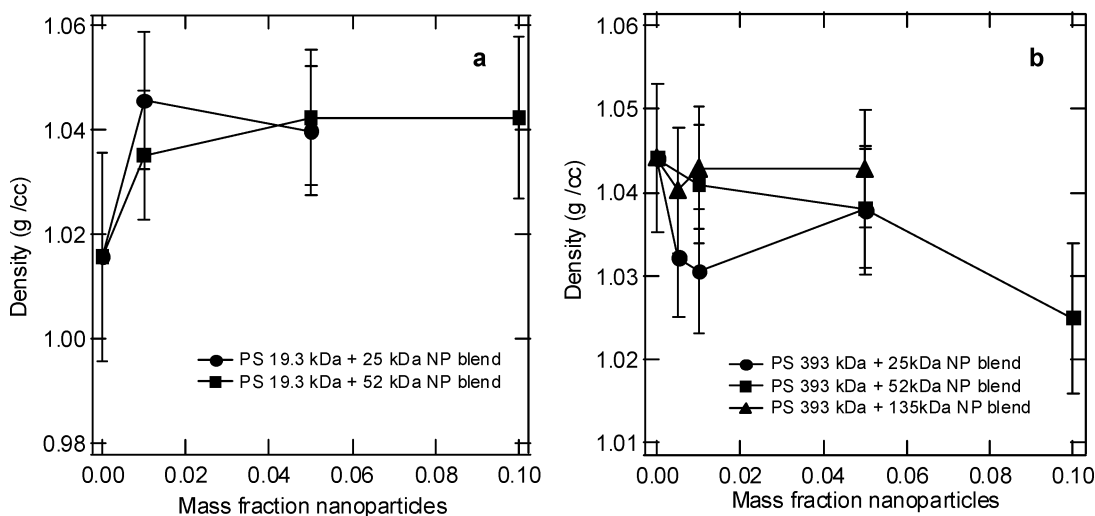
Figure 8. Bulk density variation as a function of nanoparticle concentration for PS 19.3 kDa blends (a) and PS 393 kDa blends (b) at 25 °C. For polymer molecular below M_c, the density increases, and when it is above M_c, the density decreases or remains constant, on nanoparticle addition.

least to first order. As the molecular weight of the nanoparticles decreases, for the same volume fraction, the total number of nanoparticles in the blend increases. For $\phi = 0.01$, the number of 25 kDa NP is 2.3×10^{14} NP/ mg; for the 52 kDa NP, with $\phi = 0.1$, the number of nanoparticles is 9×10^{14} NP/ mg, while for the 135 kDa NP, at $\phi = 0.2$, the number of nanoparticles is 8.6×10^{14} NP/mg. Thus, when the total number of nanoparticles present in the blend are below a certain threshold ($\sim 10^{15}$ NPs/mg), only the zero shear viscosity is reduced; however, on the addition of more nanoparticles, a reduction in viscosity at all frequencies is seen. We find that the number of polymer chains in these blends are also $\sim 10^{15}$ chains/mg and so by this empirical observation the data suggests that the chain dynamics are severely affected and the viscosity is decreased at all frequencies when the number of polymer chains approximately equals the number of nanoparticles.

The complex viscosity and the storage modulus for the blends of PS 19.3 kDa and 52 kDa NP as a function of frequency are shown in Figure 7. It can be seen that both the viscosity and storage modulus increase at all frequencies on the addition of the nanoparticles. Also, the increase in these properties scales with the concen-

tration of the added nanoparticles. The effects observed here may be due to a density increase (Figure 8a) and free volume decrease (T_g increases, Table 3) provided by the nanoparticles. Interestingly, a zero shear viscosity can be observed for all the blends measured, even though the pure nanoparticles behave as a gel (as seen in Figure 5). On comparing the data in Figure 7 with the data shown in Figure 5 for an entangled polymer, the importance of chain entanglements in the polymer is again emphasized.

The molecular mass between chain entanglements, M_e, for narrow dispersity polymer melts can be estimated by using the equation[1,60]

$$M_e = \rho R T / G_N \qquad (8)$$

where ρ is the bulk density of the material at temperature T and R is the ideal gas constant. The bulk density values for the various PS 19.3 kDa and PS 393 kDa blends are shown in Figure 8. It can be seen that the addition of the nanoparticles may cause a very small reduction in the bulk density for PS 393 kDa blends, particularly for the smaller nanoparticles (Figure 8b). From Table 2, it is observed that the plateau modulus

Table 3. The Viscosity Ratio, under Terminal Conditions, Glass Transition Temperature, and Degree of Confinement for the Pure Nanoparticles, Linear Polystyrenes, and Their Blends

nanoparticle blend	viscosity ratio	T_g (°C)	R_g/h	nanoparticle blend	viscosity ratio	T_g (°C)	R_g/h
PS 25.3 kDa NP		96.8		PS 75 kDa	1.0	106.3	0
PS 52 kDa NP		107.5		PS 75 kDa + 0.5% 25 kDa NP	0.93	106.2	0.88
PS 135 kDa NP		131.5		PS 75 kDa + 1.0% 25 kDa NP	0.91	106.0	1.19
PS 19.3 kDa	1.0	99.5	0	PS 75 kDa + 5.0% 25 kDa NP	0.91	106.5	2.66
PS 19.3 kDa + 1.0% 25 kDa NP	1.22	101.4	0.60	PS 75 kDa + 10% 25 kDa NP	0.73	106.6	4.16
PS 19.3 kDa + 5.0% 25 kDa NP	1.65	101.4	1.34	PS 75 kDa + 0.5% 52 kDa NP	1.44	105.0	0.69
PS 19.3 kDa + 10% 25 kDa NP	1.73	102.0	2.10	PS 75 kDa + 1.0% 52 kDa NP	1.59	106.1	0.93
PS 19.3 kDa + 1.0% 52 kDa NP	1.55	101.4	0.47	PS 75 kDa + 5.0% 52 kDa NP	0.60	104.7	2.10
PS 19.3 kDa + 5.0% 52 kDa NP	1.86	101.3	1.05	PS 75 kDa + 20% 52 kDa NP	0.89	104.0	5.93
PS 19.3 kDa + 10% 52 kDa NP	1.75	100.9	1.65	PS 75 kDa + 0.5% 135 kDa NP	1.19	104.4	0.50
PS 19.3 kDa + 30% 52 kDa NP	3.61	103.4	4.91	PS 75 kDa + 1.0% 135 kDa NP	1.33	106.5	0.68
PS 31.6 kDa	1.0	104.5	0	PS 75 kDa + 5.0% 135 kDa NP	1.05	106.3	1.52
PS 31.6 kDa + 0.5% 25 kDa NP	0.97	103.0	0.61	PS 393 kDa	1.0	106.9	0
PS 31.6 kDa + 1.0% 25 kDa NP	1.03	104.2	0.83	PS 393 kDa + 0.5% 25 kDa NP	0.41	106.1	2.02
PS 31.6 kDa + 5.0% 25 kDa NP	1.08	104.0	1.36	PS 393 kDa + 1.0% 25 kDa NP	0.20	104.1	2.72
PS 31.6 kDa + 1.0% 52 kDa NP	1.03	103.2	0.58	PS 393 kDa + 0.5% 52 kDa NP	0.58	105.9	1.58
PS 31.6 kDa + 2.0% 52 kDa NP	1.05	103.3	0.77	PS 393 kDa +1.0% PS 52 kDa NP	0.50	104.9	2.13
PS 31.6 kDa + 5.0% 52 kDa NP	1.04	103.4	1.73	PS 393 kDa + 8.0% PS 52 kDa NP	0.48	96.7	6.40
				PS 393 kDa + 10% 52 kDa NP	0.21	106.2	7.47
				PS 393 kDa + 0.5% 135 kDa NP	0.53	103.5	1.15
				PS 393 kDa + 1.0% 135 kDa NP	0.58	106.0	1.55
				PS 393 kDa + 5.0% 135 kDa NP	0.64	106.6	3.48
				PS 393 kDa + 20% 135 kDa NP	0.18	106.0	9.60

is unaffected by the 52 and 135 kDa nanoparticle addition at lower volume fractions. Hence, for those samples, the relation in eq 8 implies that M_e remains unaffected by nanoparticle addition. From Figure 4b, it can be seen that, for the 52 kDa NP at $\phi = 0.08$, the terminal viscosity decreases by about 60% with nanoparticle addition. Thus, even with this large reduction in viscosity, the polymer entanglements are not affected, at least in the way entanglements are thought of traditionally. This is surprising behavior, as the effects on viscosity produced by nanoparticle addition are strongly dependent on the presence or absence of entanglements (Figures 3 and 4).

In parts a and b of Figure 9, the $G''(\omega)$ data were used to obtain the continuous relaxation spectrum for PS 393 kDa and its blends with the 52 kDa NP (up to $\phi = 0.1$), as described in the Experimental Section. It can be seen that the relaxation spectra for pure polystyrene as well as the blends, have a peak near $\lambda \approx 30$ s indicative of a narrow molecular mass distribution in the polymer sample.[61] It should be noted that the pure nanoparticles have an infinite terminal relaxation time, suggesting that the relaxation properties of the nanoparticle–polymer blend are distinct and not a distribution of the individual relaxation times of its components. This observation is in contrast to what is generally observed for blends of low and high molecular mass polystyrene.[61] In addition, as no separate relaxation times are seen for the pure nanoparticles, there is no nanoparticle structure formation within the polymer melt as has been seen in a few previous nanoparticle–polymer systems.[28,62]

For $\phi = 0.1$ (Figure 9b), it can be seen that the relaxation modulus for the blends is reduced, when compared to the relaxation modulus for the pure polymer, at all relaxation times. This could be attributed to a dilution effect with the nanoparticles acting as plasticizers.[63–66] However, addition of the nanoparticles
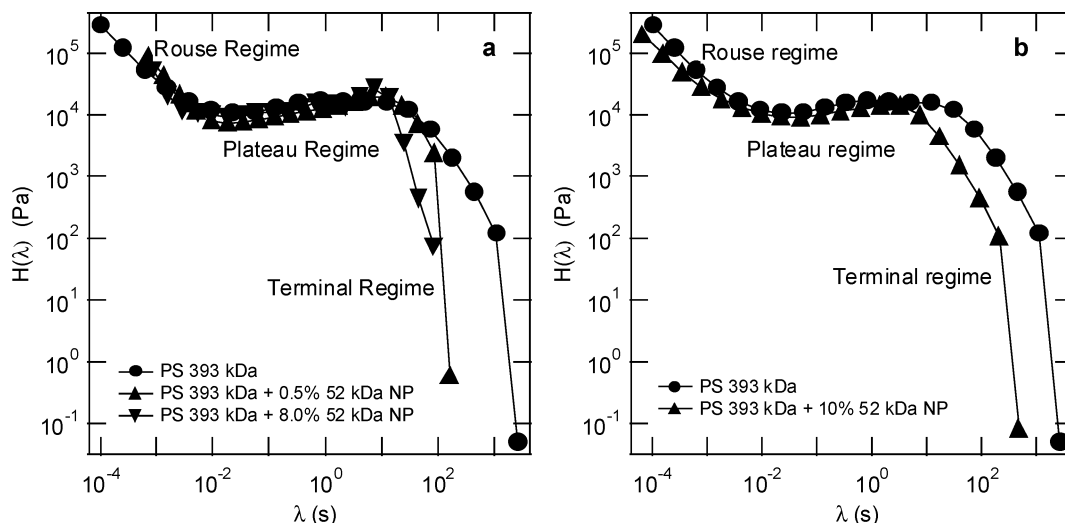
Figure 9. Relaxation spectra for pure PS 393 kDa and its blends with 52 kDa NP up to concentrations of 8% (a) and for a concentration of 10% (b). The Rouse, plateau, and terminal regimes are also shown. It can be seen that the nanoparticles only affect the terminal regime, by reducing the longest relaxation time, at lower concentrations while at higher concentrations, a reduction occurs at all relaxation times.
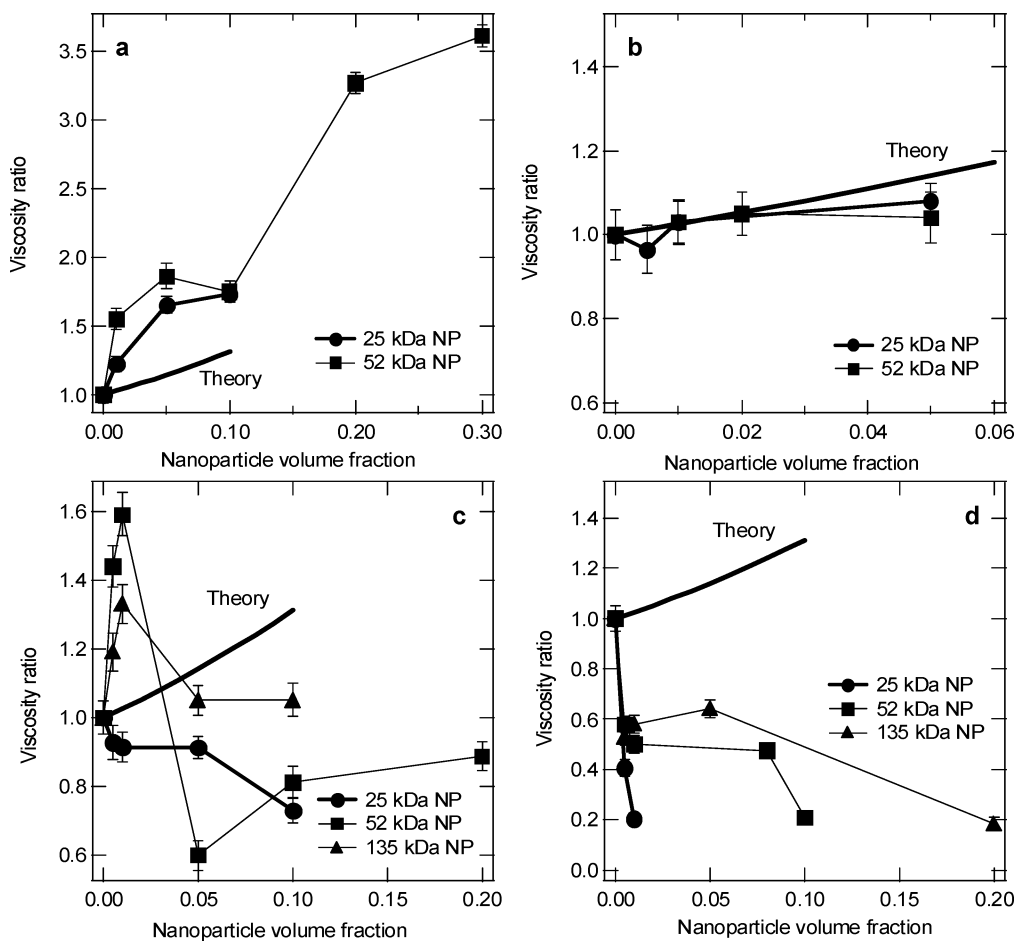
Figure 10. Viscosity ratio of the nanoparticle blends with respect to pure polystyrene as a function of nanoparticle volume fraction, with different molecular weight linear polystyrenes' at 170°C: (a) 19.3, (b) 31.6, (c) 75, and (d) 393 kDa. The curves labeled theory are the values predicted by Batchelor's relation for this system, ending at the limit of the relation's applicability ($\phi \sim 0.1$).

at low volume fractions (up to $\phi = 0.08$, Figure 9a), quite unexpectedly, does not significantly affect the Rouse or the plateau regime of the relaxation spectra. Instead, nanoparticle addition reduces only the longest relaxation times (terminal region) for the polymer chain, causing a fall in the terminal viscosity. These are the relaxations caused by the reptation[7,67] of a polymer chain in the polymer melt.

There are several mechanisms that may cause this curious behavior. We hypothesized in our previous publication that a reduction in viscosity is produced by an increase in free volume, for a given temperature, due to a reduction in the glass transition temperature found in many of the blends discussed here. This is part of the reason for the viscosity decrease; however, as seen in Table 3 a clear correlation between glass transition temperature and viscosity reduction is not apparent with this expanded data set. Furthermore, there is no clear glass transition reduction when R_g/h is greater than one, see Figure 4a, and a viscosity reduction is evident. Thus, another mechanism must exist to explain the viscosity reduction and possibly operate in tandem to the free volume change (see Figure 8b).

We hypothesize that these phenomena are related to the double reptation[68,69] or constraint release[70] phenomenon introduced by the nanoparticles. In this model, constraints are released due to movement of surrounding molecules constituting the entanglement mesh (tube[7]). This has the effect of reducing the relaxation

time, yet, not the modulus, as we observe experimentally.

The physics of the mechanism introduced by the nanoparticles will certainly depend on the relative diffusion time scales of the nanoparticle and polymer. As evident from Figure 9, the pure 393 kDa polymer relaxation time is of order 10−50 s. Assuming the nanoparticles follow the SE model one can estimate a diffusion time, through a distance a, as ∼50 s (=$\zeta a^2/k_B$T, k_B is Boltzmann's constant) which is on the same order as the polymer relaxation time. One may expect a viscosity reduction if the nanoparticles diffuse much more rapidly than the linear polymer so they cannot contribute to the entanglement mesh. So, the continuum SE relation may not be valid for nanoparticles diffusing through the polymer (temporary) network to allow this hypothesized mechanism. Diffusion of neutraly interacting NPs in entangled melts is certainly worthy of further study and here we merely (tentatively) hypothesize that the NPs invoke constraint release noting inconsistencies of this model with some of the data.

Yet, once there are approximately the same number of nanoparticles and polymer molecules per unit volume the viscosity falls at all frequencies. Clearly, under this condition, the entanglement network or tube of constraints has suffered to great extent and the plateau modulus is seen to decrease. However, this curious phenomenon occurs in the high frequency Rouse regime that is not affected at all until this nanoparticle

concentration. So, once the entanglement network is severely affected, to reduce the plateau modulus and viscosity at all frequencies, the Rouse regime is similarly affected. We find all these observations remarkable and postulate that what we interpret as independent free volume and constraint release mechanisms in fact operate in concert to generate the flow property modification.

Conclusion

We have shown that addition of polystyrene nanoparticles to linear polystyrene produces peculiar and unique behavior with a viscosity reduction only when the polymer molecule is entangled and confined. In fact, there appears to be critical behavior at the characteristic molecular mass for entanglements where the viscosity does not change, within experimental error. Furthermore, when there is approximately one nanoparticle present for each polymer molecule, an abrupt viscosity decrease is present at all frequencies.

In our previous study,[29] we demonstrated that the increase in free volume, signaled by a glass transition temperature decrease, accounted for the viscosity reduction at a given temperature. Here we have extended the data set to realize the phenomenon is much more complicated with a viscosity increase present when the polymer molecule is not confined then a precipitous drop occurs upon molecular confinement. Furthermore, the plateau modulus is not initially affected suggesting no change in the number of entanglements. We hypothesize that the nanoparticles induce constraint release affecting the longest relaxation modes thereby producing a terminal viscosity decrease without reduction in the plateau modulus. However, as the nanoparticle concentration is increased, until there is approximately one nanoparticle for every polymer molecule, the viscosity at all frequencies falls, as does the plateau modulus, suggesting a drastic change in the entanglement structure. Yet, the Rouse regime is similarly affected promoting the idea that the single molecule as well as the entanglement dynamics are similarly changed.

In Figure 1 we showed that when no entanglements are present then the viscosity can deviate from the Rouse prediction due to free volume effects, while reduction of entanglements above the critical molecular weight can yield a viscosity change. It appears this explanation where the two regimes are considered separately may be too simple. Above the critical molecular weight one may have free volume and entanglement changes induced by nano-objects which are not easily reconciled under existing theoretical considerations. It is clear, however, that this is a nanoscale effect and larger particle sizes will not produce any of this behavior.

Appendix

Here we present the viscosity ratio for the blends given in Figures 3 and 4 as a function of volume fraction in Figure 10. It is clear there is no scaling with volume fraction as expected for suspensions.

References and Notes

(1) Ferry, J. D. *Viscoelastic properties of polymers*, 3rd ed.; J. Wiley & Sons: New York, 1980.
(2) Fox, T. G.; Flory, P. J. *J. Am. Chem. Soc.* **1948**, *70*, 2384−2395.
(3) Fox, T. G.; Flory, P. J. *J. Polym. Sci.* **1954**, *14*, 315−319.
(4) Berry, G. C.; Fox, T. G. *Adv. Polym. Sci.* **1968**, *5*, 261−357.
(5) Mackay, M. E.; Henson, D. J. *J. Rheol.* **1998**, *42*, 1505−1517.
(6) Rouse, P. E. *J. Chem. Phys.* **1953**, *21*, 1272−1280.
(7) deGennes, P. G. *J. Chem. Phys.* **1971**, *55*, 572−579.
(8) Doi, M.; Edwards, S. F. *The theory of polymer dynamics.* Clarendon Press: Oxford, U.K., 1986.
(9) Lodge, T. P.; Rotstein, N. A.; Prager, S. *Adv. Chem. Phys.* **1990**, *79*, 1−132.
(10) Kotliar, A. M.; Kumar, R.; Back, R. A. *J. Polym. Sci., Part B: Polym. Phys.* **1990**, *28*, 1033−1045.
(11) Liu, C.-Y.; Morawetz, H. *Macromolecules* **1988**, *21*, 515−518.
(12) Farrington, P. J. Polymer structure, dynamics and viscoelasticity. Ph.D. Thesis, The University of Queensland, Brisbane, 1996.
(13) Tsenoglou, C. *Macromolecules* **2001**, *34*, 2148−2155.
(14) Ianniruberto, G.; Marrucci, G. *J. Non-Newtonian Fluid Mech.* **2000**, *95*, 363−374.
(15) Zax, D. B.; Yang, D. K.; Santos, R. A.; Hegemann, H.; Giannelis, E. P.; Manias, E. *J. Chem. Phys.* **2000**, *112*, 2945−2951.
(16) Anastasiadis, S. H.; Karatasos, K.; Vlachos, G.; Manias, E.; Giannelis, E. P. *Phys. Rev. Lett.* **2000**, *84*, 915−918.
(17) Brown, H. R.; Russell, T. P. *Macromolecules* **1996**, *29*, 798−800.
(18) Jones, R.; Kumar, S.; Ho, D.; Briber, R.; Russell, T. *Macromolecules* **2001**, *34*, 559−567.
(19) Metzner, A. B. *J. Rheol.* **1985**, *29*, 739−775.
(20) Einstein, A. *Ann. Phys. Leipzig* **1906**, *19*, 371−381.
(21) Russel, W. B.; Saville, D. A.; Schowalter, W. R. *Colloidal Dispersions*; Cambridge University Press: Cambridge, U.K., 1989.
(22) Cheng, P. Y.; Schachman, H. K. *J. Polym. Sci.* **1955**, *16*, 19−30.
(23) VanDerWerff, J. C.; Kruif, C. G. d. *J. Rheol.* **1989**, *33*, 421−454.
(24) Edward, J. T. *J. Chem. Educ.* **1970**, *47*, 261−270.
(25) Lin, T.-H.; Phillies, G. D. J. *Macromolecules* **1984**, *17*, 1686−1691.
(26) Lu, Q.; Solomon, M. J. *Phys. Rev. E* **2002**, *66*, 061504.
(27) Roberts, C.; Cosgrove, T.; Schmidt, R.; Gordon, G. *Macromolecules* **2001**, *34*, 538−543.
(28) Zhang, Q.; Archer, L. A. *Langmuir* **2002**, *18*, 10435−10442.
(29) Mackay, M. E.; Dao, T. T.; Tuteja, A.; Ho, D. L.; Horn, B. v.; Kim, H.-C.; Hawker, C. J. *Nature Mater.* **2003**, *2*, 762−766.
(30) Harth, E.; VanHorn, B.; Lee, V. Y.; Germack, D. S.; Gonzales, C. P.; Miller, R. D.; Hawker, C. J. *J. Am. Chem. Soc.* **2002**, *124*, 8653−8660.
(31) Israelachvili, J. N. *Intermolecular and Surface Forces.* 2nd ed.; Academic Press: New York, 1992; p 450.
(32) Merkel, T. C.; Freeman, B. D.; Spontak, R. J.; He, Z.; Pinnau, I.; Meakin, P.; Hill, A. J. *Science* **2002**, *296*, 519−522.
(33) Cosgrove, T.; Griffiths, P. C.; Lloyd, P. M. *Langmuir* **1995**, *11*, 1457−1463.
(34) Lekkerkerker, H. N. W.; Poon, W. C.-K.; Pusey, P. N.; Stroobants, A.; Warren, P. B. *Europhys. Lett.* **1992**, *20*, 559−564.
(35) Cotton, J. P.; Decker, D.; Benolt, H.; Farnoux, B.; Higgins, J.; Jannink, G.; Ober, R.; Picot, C.; desCloizeaux, J. *Macromolecules* **1974**, *7*, 863−872.
(36) Du, F. M.; Fischer, J. E.; Winey, K. I. *J. Polym. Sci., Part B: Polym. Phys.* **2003**, *41*, 3333−3338.
(37) Horio, M.; Fujii, T.; Onogi. *J. Phys. Chem.* **1964**, *68*, 778.
(38) Mead, D. W. *J. Rheol.* **1994**, *38*, 1769−1795.
(39) Mead, D. W. *J. Rheol.* **1997**, *40*, 633−661.
(40) Baumgaertel, M.; Winter, H. H. *J. Non-Newtonian Fluid Mech.* **1992**, *44*, 15−36.
(41) Thiyagarajan, P. U.; V.; Littrell, K.; Ku, C.; Wozniak, D. G.; Belch, H.; Vitt, R.; Toeller, J.; Leach, D.; Haumann, J. R.; Ostrowski, G. E.; Donley, L. I.; Hammonds, J.; Carpenter, J.

M.; Crawford, R. K. *ICANS XIV−The Fourteenth Meeting of the International Collaboration on Advanced Neutron Sources*; June 14−19, 1998, Starved Rock Lodge: Utica, IL, 1998, Vol. 2, pp 864−878.

(42) Thiyagarajan, P.; Epperson, J. E.; Crawford, R. K.; Carpenter, J. M.; Klippert, T. E.; Wozniak, D. G. *J. Appl. Crystallogr.* **1997**, *30*, 280−293.

(43) Debye, P. *Phys. Colloid Chem.* **1947**, *51*, 18−32.

(44) King, S. M. Small-angle neutron scattering. In *Modern Techniques for Polymer Characterisation*; Pethrick, R. A., Dawkins, J. V.; Eds.; John Wiley & Sons: New York, 1999.

(45) Glasstone, S.; Laidler, K. J.; Eyring, H. *The theory of rate processes*; McGraw-Hill Book Co.: New York, 1941.

(46) Higgins, J. S.; Benoît, H. C. *Polymers and neutron scattering*; Clarendon Press: Oxford, U.K., 2002.

(47) Tande, B. M.; Wagner, N. J.; Mackay, M. E.; Hawker, C. J.; Vestberg, R.; Jeong, M. *Macromolecules* **2001**, *34*, 8580−8585.

(48) Weng, D.; Lee, H. K.; Levon, K.; Mao, J.; Scrivens, W. A.; Stephens, E. B.; Tour, J. M. *Eur. Polym.* J. **1999**, *35*, 867−878.

(49) Cole, D.; Shull, K.; Baldo, P.; Rehn, L. *Macromolecules* **1999**, *32*, 771−779.

(50) Guinier, A. F.; G, *Small angle scattering of X-rays.* Wiley: New York, 1955.

(51) Griffith, W. L.; Triolo, R.; Compere, A. L. *Phys. Rev. A* **1987**, *35*, 2200−2206.

(52) Batchelor, G. K. *J. Fluid Mech.* **1977**, *83*, 97−117.

(53) Antonietti, M.; Pakula, T.; Bremser, W. *Macromolecules* **1995**, *28*, 4227−4233.

(54) Antonietti, M.; Bremser, W.; Muschenborn, D.; Rosenauer, C.; Schupp, B.; Schmidt, M. *Macromolecules* **1991**, *24*, 6636.

(55) Onogi, S.; Masuda, T.; Kitagawa, K. *Macromolecules* **1970**, *3*, 109−115.

(56) Onogi, S.; Kato, H.; Ueki, S.; Ibaragi, T. *J. Polym. Sci.: Part C* **1966**, *15*, 481−494.

(57) Lomellini, P. *Polymer* **1992**, *33*, 1255−1260.

(58) Tsenoglou, C. *J. Polym. Sci., Part B: Polym. Phys.* **1988**, *26*, 2329.

(59) Wu, S. *Polymer* **1987**, *28*, 1144.

(60) Graessley, W. W. *The Entanglement Concept in Polymer Rheology*; Springer-Verlag: New York, 1974; Vol. 16.

(61) Masuda, T.; Kitagawa, K.; Inoue, T.; Onogi, S. *Macromolecules* **1970**, *3*, 116−125.

(62) Bohm, G. G. A.; Nguyen, M. N. *J. Appl. Polym. Sci.* **1995**, *55*, 1041−1050.

(63) Roberts, C.; Cosgrove, T.; Schmidt, R. G.; Gordon, G. V. *Macromolecules* **2001**, *34*, 538−543.

(64) Kopesky, E. T.; Haddad, T. S.; Cohen, R. E.; McKinley, G. H. *Macromolecules* **2004**, *37*, 8992−9004.

(65) Nuel, L.; Denn, M. M. *Rheol. Acta* **1991**, *30*, 65−70.

(66) Lakdawala, K.; Salovey, R. *Polym. Eng. Sci.* **1987**, *27*, 1043−1049.

(67) Larson, R. G. *The Structure and Rheology of Complex Fluids.* Oxford University Press: New York, 1999.

(68) des Cloizeaux, J. D. *Europhys. Lett.* **1988**, *5*, 437−442.

(69) des Cloizeaux, J. *Makromol. Chem., Macromol. Symp.* **1991**, *45*, 153−167.

(70) Tsenoglou, C. *Macromolecules* **1991**, *24* (8), 1762−1767.